Advances in Geo-Energy Research

Vol. 7, No. 2, p. 99-110, 2023

Original article

# Investigation of fractured carbonate reservoirs by applying shear-wave splitting concept

Alejandro Diaz-Acosta[1], Fateh Bouchaala[1]*, Tadahiro Kishida[2], Mohamed S. Jouini[3], Mohammed Y. Ali[1]

[1]*Department of Earth Sciences, Khalifa University, Abu Dhabi 127788, UAE*

[2]*Department of Civil Infrastructure and Environmental Engineering, Khalifa University, Abu Dhabi 127788, UAE*

[3]*Department of Mathematics, Khalifa University, Abu Dhabi 127788, UAE*

**Keywords:**
Fractures
vertical seismic profiling
shear wave splitting
velocity analysis

**Cited as:**
Diaz-Acosta, A., Bouchaala, F., Kishida, T., Jouini, M. S., Ali, M. Y. Investigation of fractured carbonate reservoirs by applying shear-wave splitting concept. Advances in Geo-Energy Research, 2023, 7(2): 99-110.
https://doi.org/10.46690/ager.2023.02.04

**Abstract:**
In this study, fracture orientations in carbonate reservoirs were determined using a multicomponent velocity analysis based on shear wave splitting. The analysis is based on the estimated velocities of large seismic events with different polarizations. In a fractured zone with a dominant orientation, weak amplitude split shear events, including shear noise, result in shear waves that are polarized toward the symmetry and anisotropy axes and propagate with a common fast and slow velocity, respectively. Thus, a velocity stack should show high coherency anomalies in directions parallel and orthogonal to the fracture strike. Furthermore, because the analysis is applied locally at a specific depth range, it is less susceptible to the effects of overburden anisotropy and noise. The dominant fracture orientations from carbonate reservoirs of four oilfields were compared to those interpreted from fullbore microimager and core data. Fractures in two offshore reservoirs strike NNE-SSW and NW-SE, which are related to Zagros stress. Fractures in two onshore reservoir strikes NE-SW, while in deeper onshore reservoir fractures are aligned with N-S direction. The findings of this study are promising, particularly for the fractured reservoirs especially those located in Abu Dhabi, which are characterized by high heterogeneity and complex fracture network related to complex tectonic history. In order to obtain geometrical parameters of fractures at seismic scale, it is recommended to implement the analysis adapted in this study after acquiring three component zero-offset vertical seismic profiling.

## 1. Introduction

Natural fractures strongly control the hydraulic properties of saturated rocks. Therefore, estimation of geometrical properties of fractures are crucial to accurately assess permeability and understand fluid flow in the reservoir zones. These details are necessary for reservoir monitoring, production rate estimation, dynamic simulation and enhanced oil recovery. Several numerical models have been developed to estimate fracture properties from seismic data. Bakulin et al. (2000) conducted a numerical study to investigate relationship between anisotropy parameters derived from surface seismic data and fracture properties. Zhao et al. (2016) suggested that the spatial distribution of pores and cracks should be incorporated for an accurate prediction of the effective elastic parameters based on numerical study on the elastic interaction between pores and cracks. However, real data are more challenging to work with than synthetic data, particularly in complex media like carbonate rocks. The geometrical and physical properties of reservoirs can be determined from field data using a variety of techniques based on different concepts. Interpretation of fullbore microimager (FMI) and core data are commonly used to obtain geometrical properties of fractures at well location. Curvature, dip, azimuth, coherency, similarity, semblance, variance, spectral decomposition (e.g., Marfurt et al., 1998; Chopra and Marfurt, 2007; Hale, 2013; Gao and Di, 2015;

Yandy Scientific Press

*Corresponding author.
*E-mail address*: 100058334@ku.ac.ae (A. Diaz-Acosta); fateh.bouchaala@ku.ac.ae (F. Bouchaala); tadahiro.kishida@ku.ac.ae (T. Kishida); mohamed.jouini@ku.ac.ae (M. S. Jouini); mohammed.ali@ku.ac.ae (M. Y. Ali).

Received September 30, 2022; revised November 12, 2022; accepted December 6, 2022; available online December 9, 2022.

Jaglan et al., 2015; Skeith et al., 2015; Mandal and Srivastava, 2018) are the seismic attributes mostly used to derive fractures properties between wells. However, these attributes may only be able to identify the geometrical properties of fractures rather than physical ones. Full waveform inversion is a suitable tool for an accurate mapping of media with high fracture density, but with low resolution (Takougang et al., 2020). Seismic waves attenuation also, has a great potential for investigating physical properties of fractures as well (Bouchaala et al., 2019) because of its closure to petrophysical properties of reservoirs, such as fluid type and saturation (e.g., Bouchaala and Guennou, 2012; Matsushima et al., 2017). Scattering and wave-induced fluid flow, which are the main seismic attenuation mechanisms, cause a scale-dependence of seismic anisotropy in fractured media (Ding et al., 2020, 2021). However, a lack of well-established methods makes the estimate of seismic attenuation difficult.

In an anisotropic media, shear-wave splitting occurs when an incident shear wave exhibits birefringence, resulting in two shear waves that are polarized parallel and perpendicular to the fracture strike, respectively (Crampin and Peacock, 2008). The shear wave $S_1$ propagates with faster speed than $S_2$ (Bale et al., 2009). Therefore, this anisotropy related phenomenon may be described by the difference in arrival times of shear waves originated from a single source (Simm and Bacon, 2014). Tsuji et al. (2011) assessed seismic anisotropy from walkaround three component vertical seismic profiling (3C VSP) data in order to reveal the stress state within the Kumano basin. In order to do that, they processed the 3C VSP data in order to extract the main shear events and analyze shear-wave splitting. Miyazawa et al. (2008) measured shear-wave splitting by isolating down-going P- and S-waves from noise generated by human activities. However, the overburden effect and difficulty in extracting shear-waves make the application of shear-wave splitting concept in Abu Dhabi reservoirs challenging, despite the abundance of 3C seismic data. In addition to that, Abu Dhabi reservoirs are complex due to their heterogeneous lithology mainly composed of carbonate rocks.

To tackle the difficulties listed above, we have adopted a sophisticated method based on multicomponent shear-wave velocity analysis (Pevzner et al., 2011) and the shear-wave splitting concept. This method is suitable for zero-offset VSP data, and does not require the extraction of individual shear events and knowledge of their origin, which involves lot of seismic processing efforts. The method benefits from stacking of large number of weak amplitudes of any shear-events (direct, reflected, refracted, multiples, etc.) over velocity. Furthermore, this technique is less sensitive to the overburden conditions and cost-effective than walkaround VSP, FMI and coring techniques.

A workflow has been followed to apply the multicomponent velocity analysis combined with shear-wave splitting concept, starting with the rotation of horizontal component of zero-offset data. In order to optimize the numerical parameters of the technique, synthetic tests on multilayered earth models with similar properties to Abu Dhabi oilfields and varying levels of noise were performed. Furthermore, reservoir zones of two offshore and onshore oilfields were investigated in order to evaluate the potential of the current technique for detecting shear-wave splitting and obtaining orientation of fractures.

## 2. Geological and tectonic setting

Structural features of Abu Dhabi oilfields are the result of complex tectonic mechanisms, connected to the evolution of Arabian platform since Proterozoic crustal amalgamation. The Arabian Plate formed as a part of the Pangea Supercontinent, spanning from the Late Carboniferous until the Early Permian (Muttoni et al., 2009). The earliest rifting deposits in the UAE are the Early Permian rocks of Jabal Qamar at the Dibba zone, and the mid-Permian Bih Formation in Musandam Peninsula (Searle, 2007).

At the Late Cretaceous, the region exhibited a mature rifted margin with carbonate dominated rocks in a continuously expanding basin related to the Tethys Ocean opening (Ali et al., 2013). During the end of the Cenomanian ($\sim$ 93.5 Ma) there was a major break in the stability of the sedimentation due to the obduction of the SW-directed Semail ophiolite onto the eastern Arabian continental margin (Searle, 1988). The emplacement of the Semail ophiolite was completed during the early Maastrichtian ($\sim$ 70 Ma). The ophiolite complex is a thick thrust sheet (ranging from 8 to 15 km) comprising the Cenomanian oceanic crust and upper mantle (Searle et al., 2014). Due to the loading of the Upper Cretaceous passive margin of the Wasia Group, a flexural subsidence and partial erosion occurred (Ali et al., 2018). These were caused by the stacking of the obducted thrust sheets of the Semail ophiolite, and consequently the Upper Cretaceous Aruma foreland basin was created, along with a peripheral bulge at the western edge, specifically at the proximity of the obducted allochthonous units (Patton and O'connor, 1988). During the Late Oligocene-Miocene, the compressional deformation resumed after a period of a stable carbonate sedimentation (Ali et al., 2013). The deformation caused the reactivated deep-seated basement faults and development of thrust-and-fold-belt and Pabdeh foreland basin (Ali et al., 2008). This deformation belt has been interpreted as a result of the initial Zagros phase of continent-continent collision (Searle, 1988).

Abu Dhabi reservoirs are highly fractured (e.g., Sirat et al., 2007; Ali et al., 2021), hence, their porosity and hydraulic conductivity are mainly controlled by fracturing systems, making evaluation of their geometrical properties very important. Moreover, carbonates, which are renowned for their high heterogeneity and predominance in the lithology of Abu Dhabi reserves, cause intense scattering and multiple seismic noises. Therefore, applying classical shear wave splitting methods that depend on extracting the primary shear events may not be successful. A shear wave splitting method based on multicomponent shear velocity analysis will be used in order to overcome challenges in deriving orientation of fractures in carbonate rocks. This method is detailed in more depth in the section below.

## 3. Methodology

Acquiring of high-quality shear-waves, requires a source generating energy toward two horizontal orthogonal directions,

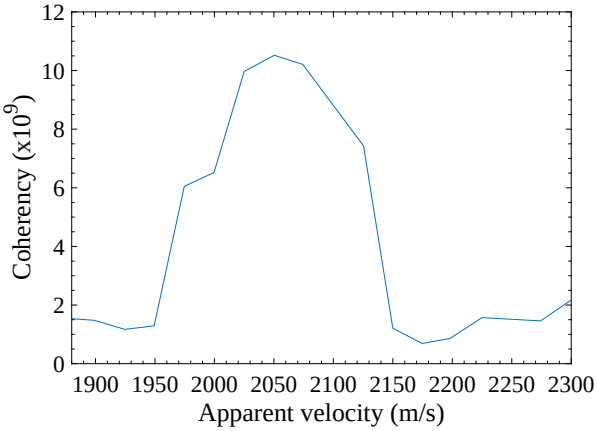


**Fig. 1**. Velocity spectrum generated by Eq. (2) at a given reference time $t_0$ and azimuth $\alpha$. The peak of the curve corresponds to the best approximation of the apparent velocity of the event.

in addition to two horizontal-component receivers. However, in practice, because of their high cost, sources that generate seismic waves that are polarized vertically are more frequently utilized in practice than sources that generate seismic waves that are polarized in the horizontal plane. Therefore, exploiting shear-waves remains more challenging than compressional ones, making a direct observation of split shear-waves in seismic data difficult. To overcome this limitation, Pevzner et al. (2011) proposed an approach based on multicomponent S-wave velocity analysis applicable on zero-offset VSP data. This approach uses many shear events instead of a few strong individual shear events, all of which have the same apparent velocity and raypath geometry. The use of the analysis within a defined sliding depth window has the advantage of reducing the impact of overburden on the reservoir zones.

In order to properly perform the analysis, a workflow consists of five main steps,

- Step 1: Rotate horizontal components $HR_1(t,z)$ and $HR_2(t,z)$ recorded within a depth interval $\triangle z$ from local receiver system toward Earth geographical system.
- Step 2: The horizontal components $HR_1(t,z)$ and $HR_2(t,z)$ obtained in geographical system coordinates are rotated toward the radial direction by using source-receiver azimuth angle $\alpha$ in the following equation:

$$H(\alpha,t,z) = HR_1(t,z)\cos\alpha + HR_2(t,z)\sin\alpha \quad (1)$$

- Step 3: A velocity spectrum (Fig. 1) at each azimuth $\alpha$ and reference time $t_0$ is generated by scanning the apparent velocity $V$ in a given range to compute a modified semblance $C$ in order to emphasize stronger events, as shown in Eq. (2):

$$C(t_0,V,\alpha) = \frac{\sum_{j=1}^{N}\left(\sum_{i=1}^{M} D_{ij}\right)^4}{M\sum_{j=1}^{N}\sum_{i=1}^{M} D_{ij}^2} \quad (2)$$

where $D_{ij}$ is calculated at the $j^{\text{th}}$ sample of the $i^{\text{th}}$ rotated trace as:

$$D_{ij} = H\left(\alpha, t_0 + \frac{\triangle z_i}{V} + \left(j - \frac{N}{2}\right)\triangle t, \triangle z_i\right) \quad (3)$$

It is noteworthy to mention that in Eq. (2), $C$ is computed along a linear travel-time line $t = t_0 + \triangle z/V$, where $\triangle z$ is the depth of a seismic trace from top of the depth interval. This is based on Landa et al. (1995) for estimating velocity from refracted data. $M$ and $N$ are the number of traces contained in the depth and time interval, respectively, $\triangle z_i$ is the distance from the top of the depth window used for the semblance computations to the depth of the $i^{\text{th}}$ trace, and $\triangle t$ is sampling time.

- Step 4: The velocity spectrum computed at one azimuth $\alpha$ and different reference times $t_0$ has to be stacked along the time axis. Then, stacked traces of all azimuths are juxtaposed in one section. The existence of two coherent events related to the fast and slow shear waves in a given depth interval, the stacked velocity spectra should display two different maxima at the fast and slow velocities, respectively, and separated by 90° along the azimuth axis.
- Step 5: By running this analysis in a moving window along the depth, a Three Dimensional (3D) volume is obtained. Velocities and azimuths at the extrema on depth slices correspond to fast and slow shear-wave velocities, and fracture strikes.

The fracture strike is identified in the proximity of the well, and corresponds to a single dominant fracture orientation. The VSP data has to be acquired in a near vertical borehole trajectory in a horizontally stratified medium. Lastly, the layers must be represented orthorhombically, including horizontal transverse isotropy (HTI) and horizontal symmetry planes.

## 4. Field datasets

The offshore oilfield I is located 80 km northwest of Abu Dhabi city (Fig. 2), where a marine walkaway VSP survey was conducted by performing 18,000 airgun shots, in an area of 3 km radius, and recorded by seventy receivers placed with a spacing of 20 m.

The data were recorded with a sampling rate of 2 ms and recording length of 4 s (Figs. 3(a) and 3(b)). The 29$^{\text{th}}$, 34$^{\text{th}}$, 49$^{\text{th}}$ and 60$^{\text{th}}$ traces were removed because of their quality due to bad receivers-ground coupling. Furthermore, the last five traces were recorded with a delay, due to an asynchronous initial recording time and an initiation of the source. The velocity analysis was performed on a near offset shot gather of 100 m. Oilfield II, is located 110 km northwest of Abu Dhabi city (Fig. 2), where zero-offset VSP data survey were carried out to record 144 levels with 15.12 m spacing, 1 ms time sampling and a recording length of 6 s (Figs. 3(c) and 3(d)). The 100$^{\text{th}}$ and 110$^{\text{th}}$ traces were removed because of their low quality. The onshore oilfield III is located south of Abu Dhabi city (Fig. 2), where zero-offset walkaway VSP data were generated by using a vibroseis. The data were recorded at 146 depth levels with a spacing of 15.24 m, with a sampling rate of 2 ms and recording length of 5 ms (Figs. 4(a) and 4(b)). Oilfield IV is located at the extreme south of Abu Dhabi, near the Saudi Arabian border (Fig. 2). A vibroseis was used to generate zero-offset VSP data, recorded at 467 levels spaced

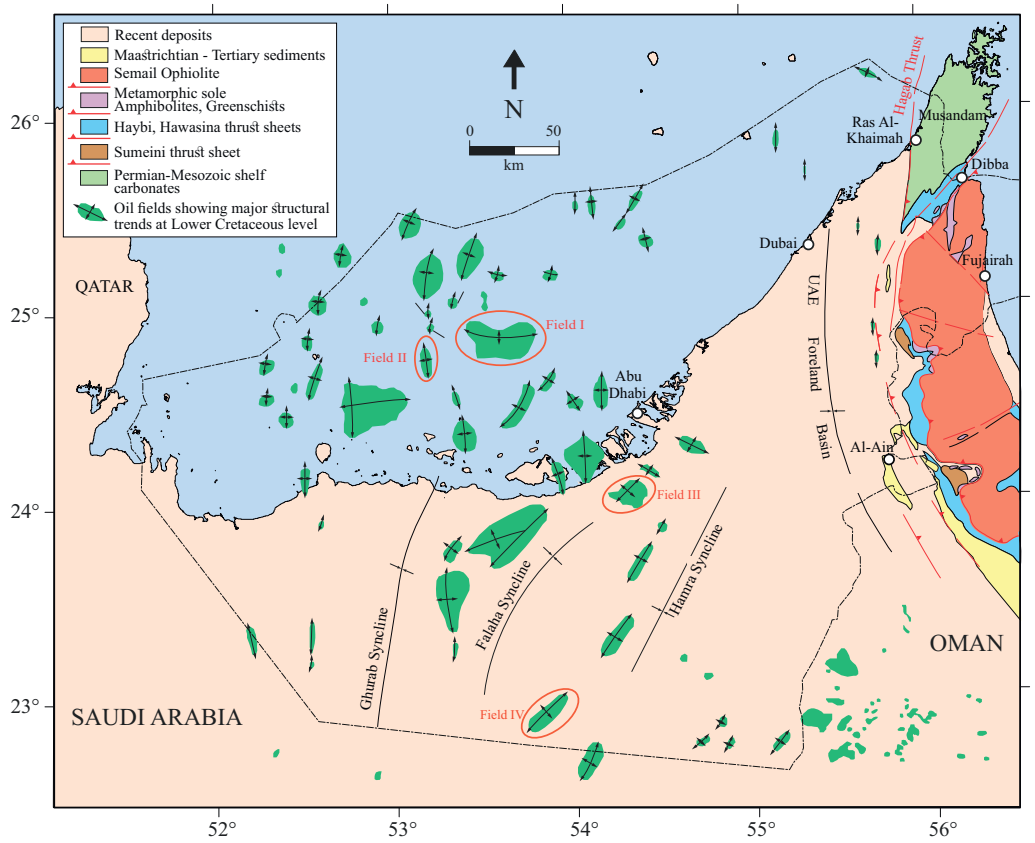


**Fig. 2**. Geographical position of the studied oilfields in the Abu Dhabi region, highlighted by red circles (modified after Bouchaala et al. (2018)).

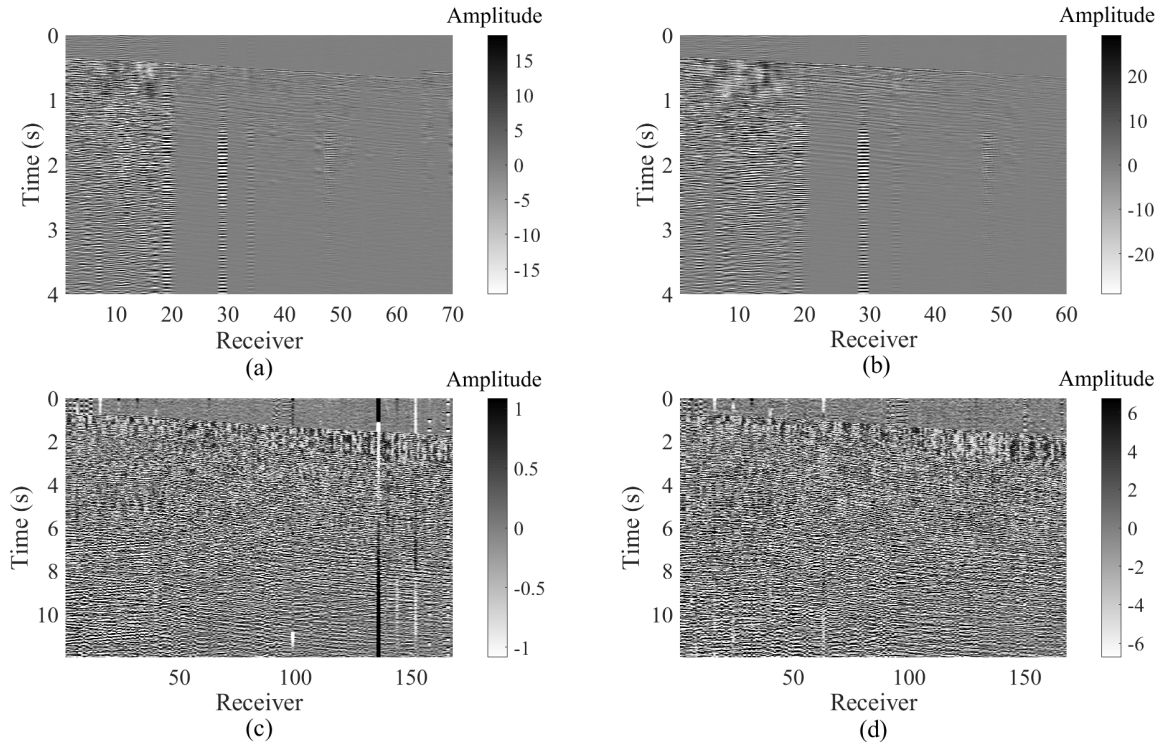


**Fig. 3**. Horizontal VSP components oriented toward, (a, c) East-West and (b, d) North-South directions recorded in the offshore oilfield I (upper row) and oilfield II (lower row).

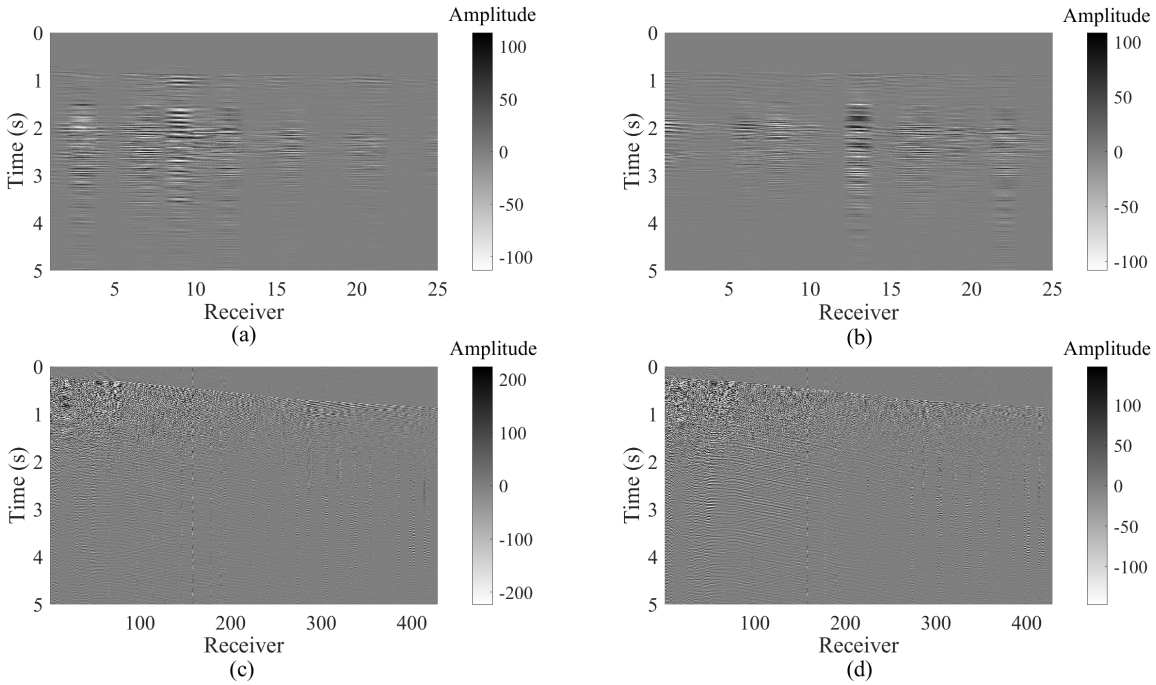


**Fig. 4**. Horizontal VSP components oriented toward, (a, c) East-West and (b, d) North-South directions recorded in the onshore oilfield III (upper row) and oilfield IV (lower row).

by 4.57 m, with a sampling rate of 2 ms and a recording length of 5 s (Figs. 4(c) and 4(d)).

## 5. Synthetic tests

The accuracy of the results of the analysis algorithm is controlled by a number of important numerical parameters, and synthetic tests are required to understand and assess these effects. Additionally, the synthetic testing allowed us to determine whether the numerical code developed for this study (Fig. 7) was ready to be applied to actual data. The code was applied on 3C VSP synthetic data generated in a multi-layered earth model having similar properties as the subsurface of both offshore and onshore oilfields. Well tops of the oilfields I and IV were used to define the layering of the multi-layered earth offshore and onshore models, respectively (Figs. 5 and 6). Check shots velocities of oilfield I were used to calculate the reflectivity and hence, to generate synthetic seismograms. The upper most layer in the offshore model corresponds to the water column. The averaged density logs in each layer in the oilfield IV, were used to generate the onshore synthetic seismograms. Velocities of the bottom layer in the two models was added as an absorption boundary, in order to satisfy the boundary conditions of the finite difference model (Bohlen, 2002).

A fast ($V_{s-off}$ = 2,350 m/s, $V_{s-on}$ = 4,468 m/s) and slow ($V_{s-off}$ = 1,600 m/s, $V_{s-on}$ = 3,468 m/s) shear-wave velocities were given along two orthogonal directions in layers located at the same depth as the reservoirs of oilfields I and IV (Figs. 5 and 6). Introducing two directional velocities, avoids the use of the computationally expensive 3D anisotropic finite-difference methods. The data were generated by using 100 bar pressure air-gun, having a Ricker signature with amplitude $r(\tau)$ described by the following equation:

$$r(\tau) = \left(1-2\tau^2\right)\exp(-\tau^2)$$
$$\tau = \pi f_c\left(t-\frac{3}{2f_c}-t_d\right) \quad (4)$$

where $t$ is propagation time, $t_d$ is delay time, $f_c$ is central frequency.

Random noise of uniform distribution was generated in the interval [a, b] by using Eq. (5), and then added to the generated synthetic seismograms with a sampling rate of 2 ms and a signal length of 4 s:

$$\text{noise} = b-(b-a)\times\text{rand}(\text{length}(X)) \quad (5)$$

where $a$ and $b$ are the minimum and maximum amplitudes of the data array $X$, respectively.

The workflow described in the Methodology section was applied on the generated synthetic seismograms, by varying the numerical parameters that control the analysis namely, increment of velocity, size of time and depth sliding windows. The results show that the error in fast and slow velocity magnitudes and the fracture strike is the lowest when time window size is around 0.06 s for both fields (Fig. 7(a)). On the other hand, a depth window around the thickness of the fractured layer (around 150 m for offshore and 300 m for onshore oilfields), captures the fracture strike and the magnitude of fast and slow velocities with high accuracy (Fig. 7(b)), with less computational cost. Lastly, the velocity step of analysis giving the best compromise between computation time and precision was chosen to be equal to 25 m/s (Fig. 7(c)). After applying the workflow of multicomponent velocity analysis, with the optimized numerical parameters, the fracture

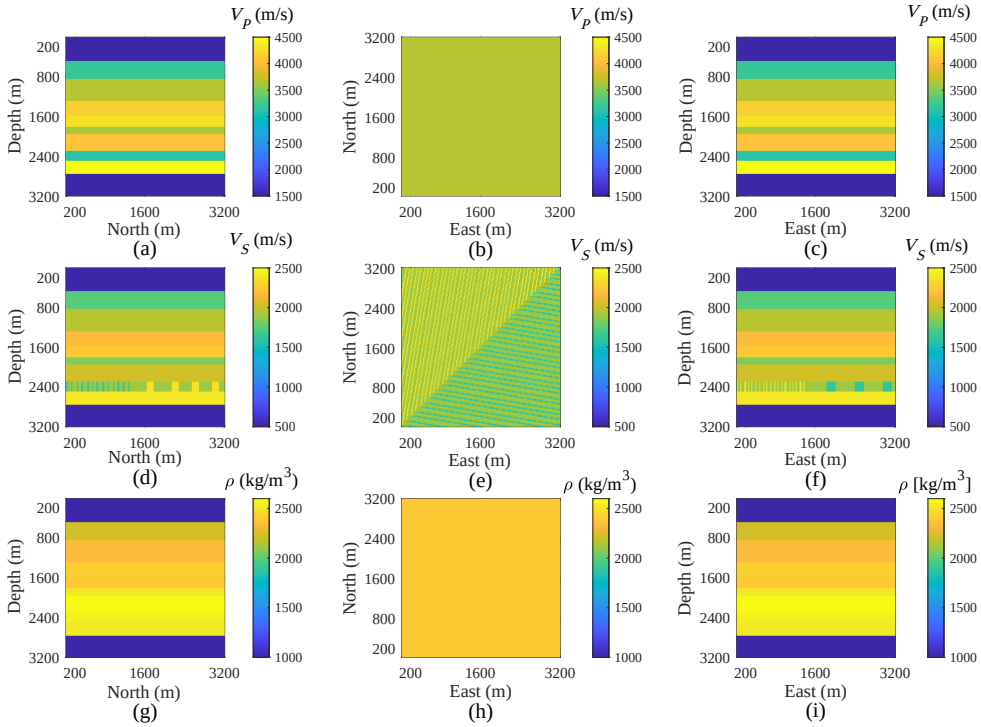


**Fig. 5**. The 3D offshore synthetic (a, b, c) compressional and (d, e, f) shear velocity models, along with (g, h, i) density ones. The first, and third column shows North-depth and East-depth cross sections, respectively, while the second column shows a slice at the reservoir zone. The magnitude of fast and slow shear velocity shown are 2,350 and 1,600 m/s, respectively.

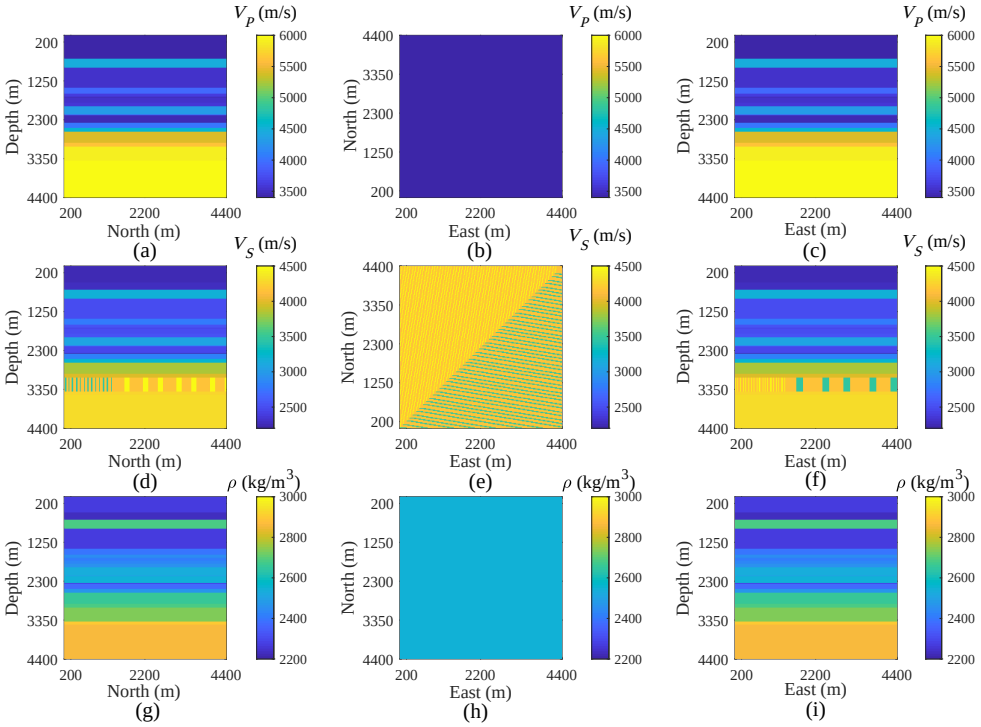


**Fig. 6**. The 3D onshore synthetic compressional (a, b, c) compressional and (d, e, f) shear velocity models, along with (g, h, i) density ones. The first and third column shows North-depth and East-depth cross sections, respectively, while the second column shows a slice at the reservoir zone. The magnitude of fast and slow shear velocity shown are 4,468 and 3,468 m/s, respectively.

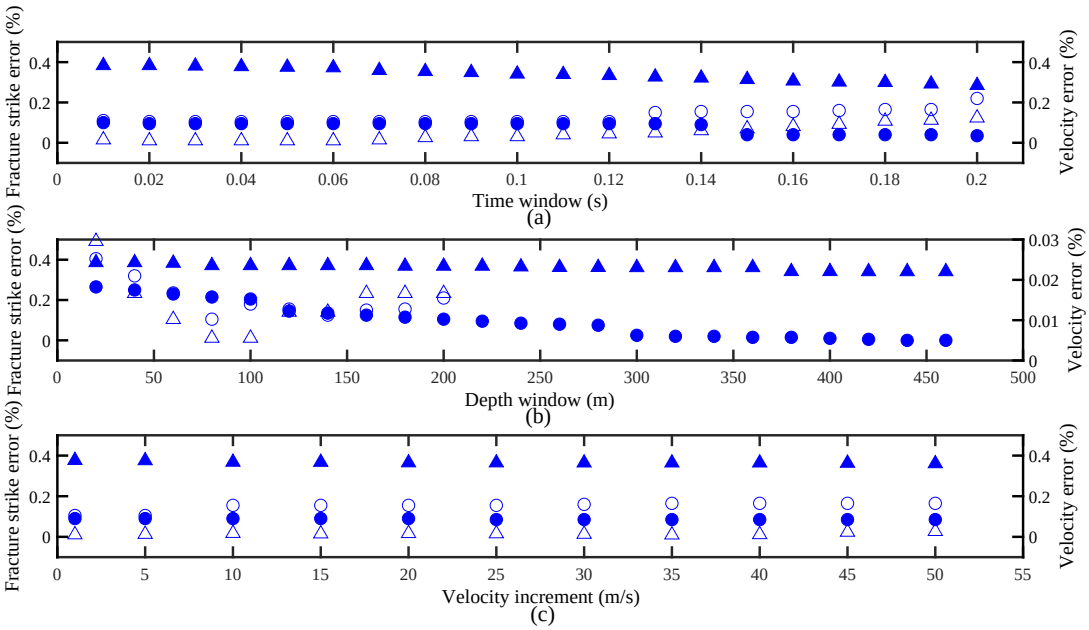


**Fig. 7**. Variation of error in fracture strike and velocity with (a) time and (b) depth windows, in addition to (c) velocity increment. The error is the difference between the input parameters of the model (strike and velocity) and the ones obtained from the multicomponent velocity analysis, the velocity error is the average of fast and slow velocity.

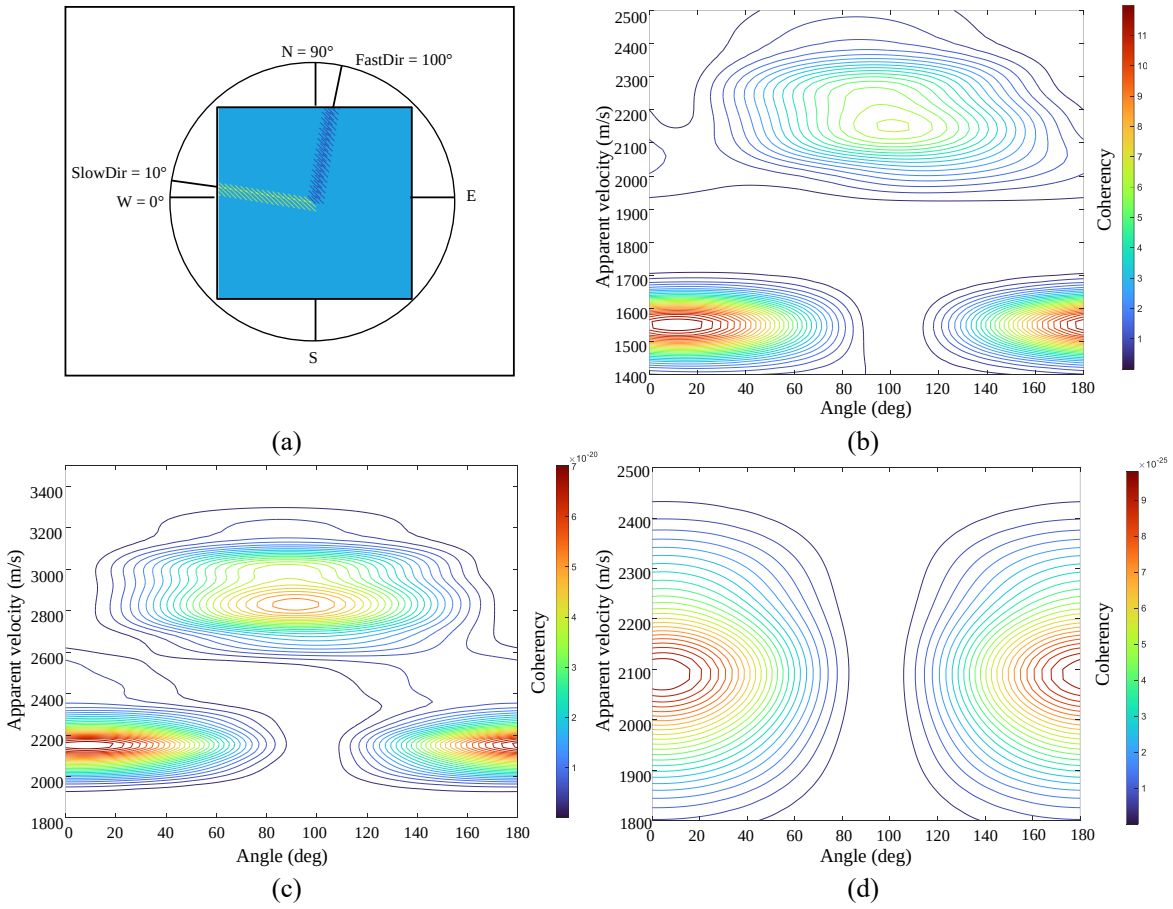


**Fig. 8**. (a) Input fast and slow directions for the synthetic models, compared to the ones obtained after applying multicomponent velocity analysis on (b) offshore and (c) onshore synthetic seismograms recorded in the fractured layer, and (d) no fractured layer.

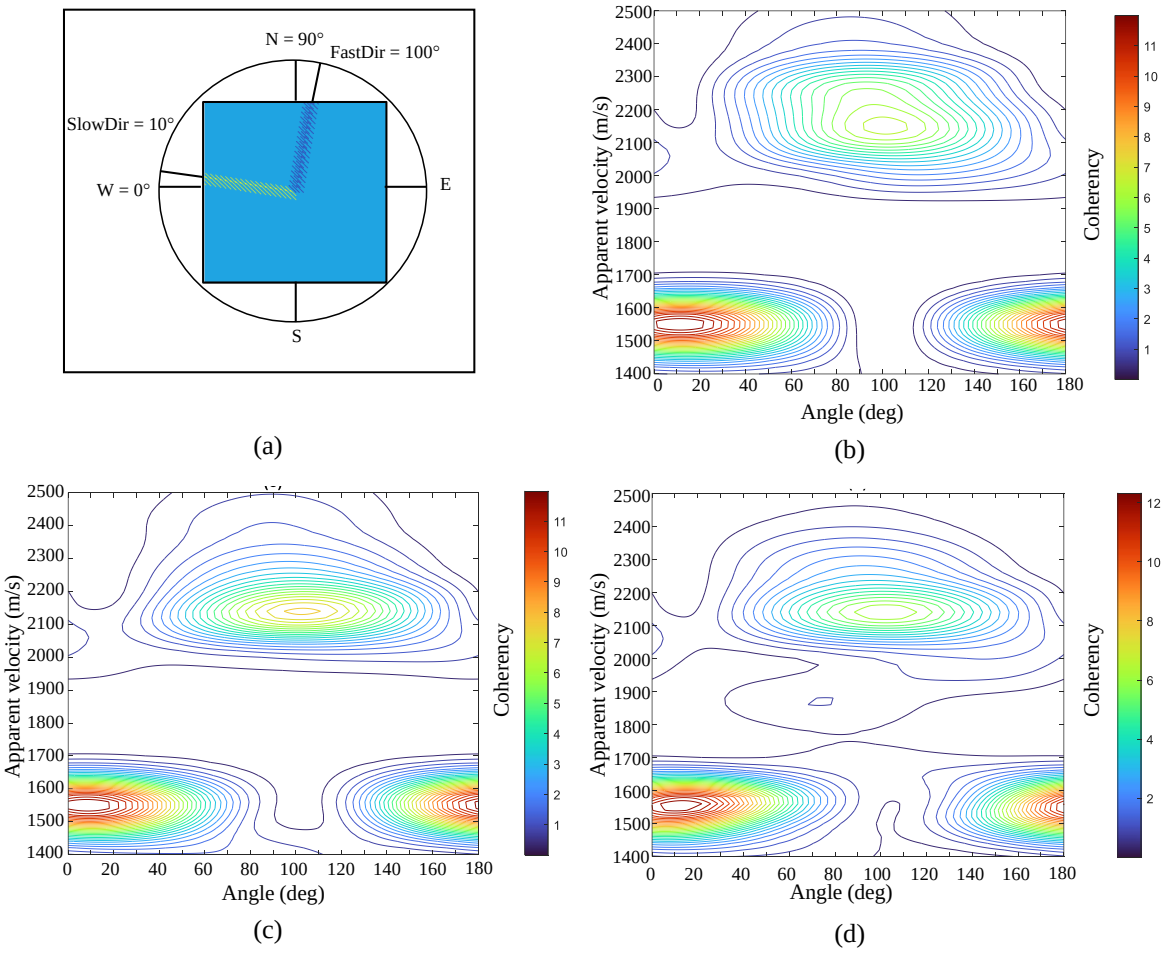


**Fig. 9**. (a) Input fast and slow directions for the synthetic models, compared to the ones obtained after applying multicomponent velocity analysis on offshore seismograms after adding (b) 5%, (c) 10% and (d) 20% noise.

strike was identified with a relative error of 3° and 25° for offshore and onshore oilfields, respectively (Figs. 8(a) to 8(c)), while the velocity was obtained with an approximate absolute value accuracy of 30 m/s and around 1,428 m/s for offshore and onshore oilfield, respectively (Figs. 8(b) and 8(c)). Although, that the onshore synthetic test steps were carefully examined, it is still difficult to explain the high error in onshore velocities. However, the objective of this study is to define the fast and slow directions, which corresponds to fracture strike and symmetry axis, respectively. The application of the multicomponent analysis method on a non-fractured media does not produce two extrema (Fig. 8(d)), meaning that the method does not produce artifacts. Furthermore, the method effectively identifies the fracture strike even when affected by uniform random noise of up to 20% of the noise calculated by Eq. (5) (Fig. 9).

## 6. Results and discussion

The multicomponent velocity analysis workflow was applied on the waveforms recorded in four oilfields. Based on synthetic test results, the time and depth windows were taken equal to 0.06 s and reservoirs thicknesses respectively, while the velocity equal to 25 m/s. The estimated fracture strikes were compared to those based on FMI interpretation at well locations.

The geological layers surrounding the four oilfields are sub-horizontal (Noufal, 2020), which is an important assumption of the applied method. At oilfield I, the oil bearing Thamama Group of Early Cretaceous age was analyzed along the measured depth interval, from 2,320 to 2,520 m (Fig. 10(a)). The identified fracture strike is of N 20° E, and the fast and slow shear-wave velocities are of 2,185 and 2,065 m/s, respectively (Figs. 10(c) and 10(e)). For oilfield-II, the reservoir zone is within the Sila Group of the Late Jurassic, specifically the Arab Formation was analyzed along the measured depth interval 3,036-3,246 m in (Fig. 10(b)). The fracture strike was identified at E 34° S, and the fast and slow shear-wave velocities are of 3,850 m/s and 3,575 m/s respectively (Figs. 10(d) and 10(f)). The obtained fracture strikes from the multicomponent velocity analysis are close to those based on the interpretation of FMI data, which validate our analysis.

The onshore oilfields (III and IV) are both contained in the NE-SW compressional fold domain (Richard et al., 2017). At oilfields III and IV, the Thamama Group is reported as reservoir zones. At oilfield III, the Habshan Formation, was

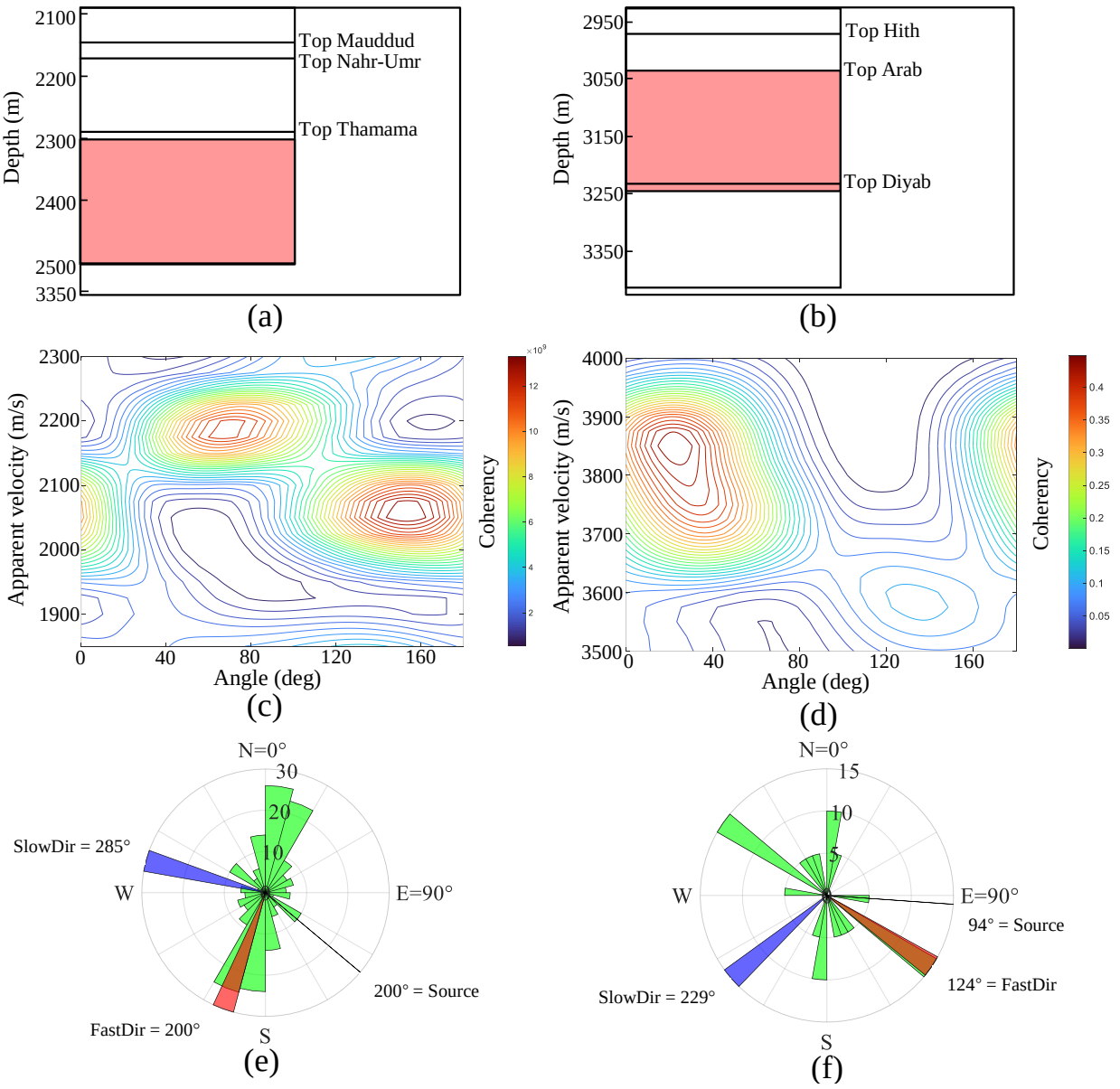


**Fig. 10**. (a, b) Interval window used for the multicomponent analysis highlighted in red, along with (c, d) azimuthal velocity spectrum, obtained at different depths and angles measured from source direction (black line). (e, f) Rose diagrams of fast (red) and slow (blue) directions obtained from multicomponent velocity analysis compared to those obtained from FMI or core interpretation (green). The left and right column display plots for offshore oilfields I and II, respectively.

analyzed along with the deepest interval of the group. The analyzed interval is from 3,243 to 3,333 m in measured depth (Fig. 11(a)).

The identified fracture strike is of N 65° W, and the fast and slow shear-wave velocities are of 3,025 and 1,850 m/s, respectively (Figs. 11(d) and 11(g)). For oilfield IV, the Kharaib, Lekhwair and Habshan belonging to Thamama Group were analyzed. The first analyzed interval contains Kharaib and Lekhwair Formations ranging in a measured depth from 2,606 to 2,690 m (Fig. 11(b)). The identified fracture strike is of N 50° E, and the fast and slow shear-wave velocities are of 3,785 and 3,400 m/s, respectively (Figs. 11(e) and 11(h)). The second analyzed interval, corresponding to the Habshan Formation, is ranging from measured depths of 3,199 to 3,374 m. The identified fracture strike is aligned with N-S direction, and the fast and slow shear-wave velocities are of 4,175 and 4,075 m, respectively (Figs. 11(f) and 11(i)). Unfortunately, FMI and core data are not available for oilfield IV.

The overall consistency between fracture orientations identified by using multicomponent velocity analysis and those obtained from the interpretation of FMI or core data collected in reservoir zones, demonstrates the great potential of this cost-effective analysis in investigating fractured reservoirs. However, to obtain reliable results synthetic tests were performed, with similar acquisition conditions as those recorded in the studied field, in order to optimize the numerical parameters

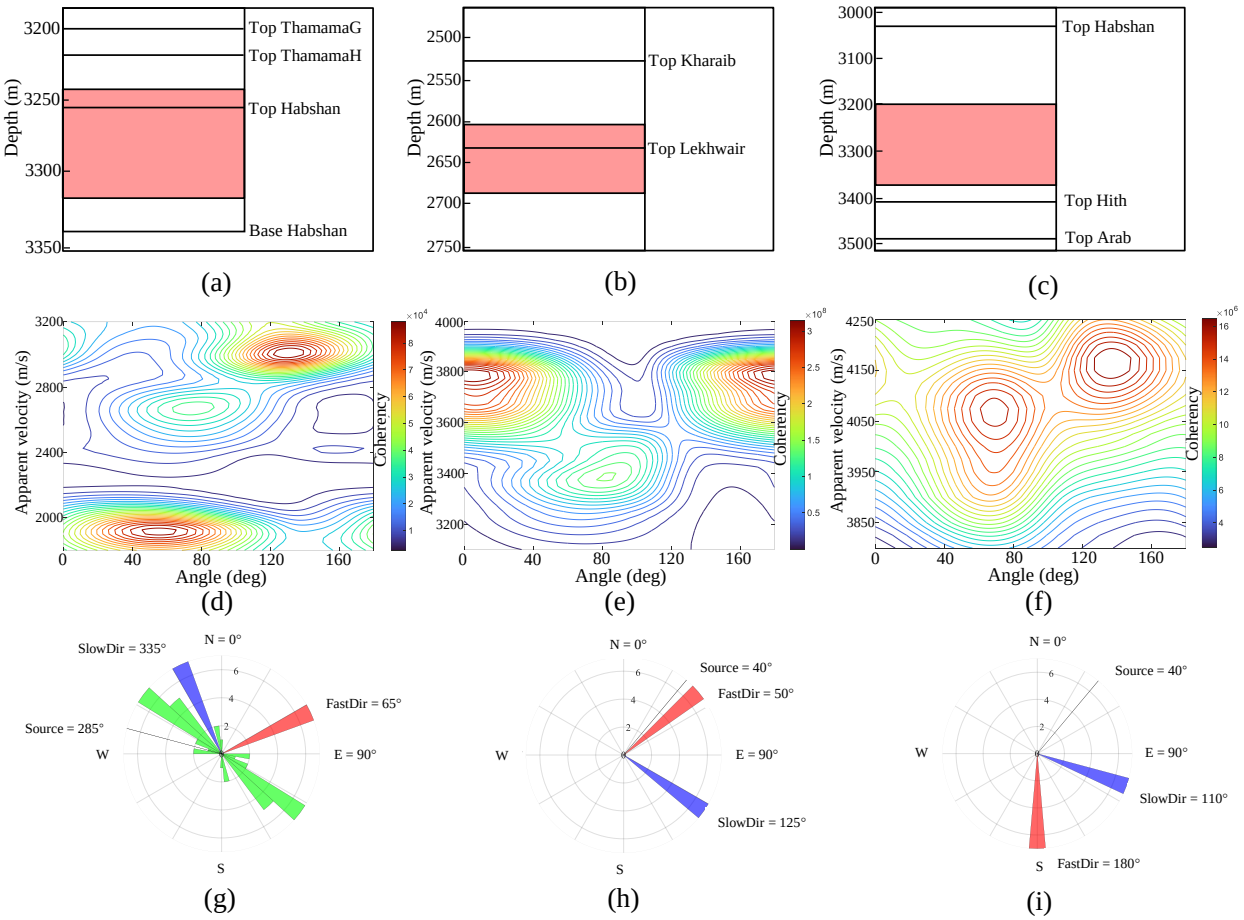


**Fig. 11**. (a, b, c) Interval window used for the multicomponent analysis highlighted in red, along with (d, e, f) azimuthal velocity spectrum, obtained at different depths and angles measured from source direction (black line). (g, h, i) Rose diagrams of fast (red) and slow (blue) directions obtained from multicomponent velocity analysis compared to those obtained from FMI or core interpretation (green). The first column display plots for onshore oilfield III, while the second and third column display plots for the upper and lower reservoirs, respectively of oilfield IV.

controlling the multicomponent analysis.

A previous shear-wave splitting study was conducted in the reservoir zone of oilfield I based on the azimuthal analysis of processed and rotated main shear events in the radial direction (Li and Ali, 2016). The results showed that the anisotropy is very weak, and the main fracture strike is N 45° E, which is different from those obtained from FMI interpretation. However, those results were not accurate because of inherent limitations in the approach, which is most probably due to the difficulty of extracting shear-waves. This demonstrates the superiority of the multicomponent analysis conducted in this study, which is based on the stack of a large number of weak magnitude shear events. The fracture orientation obtained in the reservoirs of offshore oilfields I and II, are aligned with NNE-SSW and NW-SE directions respectively, and are confirmed by FMI interpretation. These two fracture sets are extensional and formed by the Zagros stress, from the Late Eocene to present (Sirat et al., 2007). Fractures aligned with these two orientations are suggested to be predominantly steeply dipping and are open in nature (Sirat et al., 2007; Ali et al., 2021), meaning that they act as fluid conduct. The fast direction obtained in the reservoir of oilfield III is close to ENE-WSW direction, while dominant strike of fractures interpreted from FMI data is close to NW-SE direction. Such difference might be due to the small size of NW-SE fractures size compared to the wavelength of VSP waveforms, which makes the wave slightly affected by fractures aligned to this direction. Furthermore, the multicomponent analysis incorporates shear events, which propagate away from the well location; therefore, the analysis may provide dominant orientations of fractures away from the well location, where the FMI data are acquired. It is worth mentioning that fractures aligned with ENE-WSW direction, were reported by previous studies. Johnson et al. (2005) assumed that fractures striking in ENE-WSW direction, are associated with the Tethyan trend of WiMann et al. (1943), and are probably dextral faults with mixed extension and compression (Johnson et al., 2005). Fracture orientations aligned with NE-SW and N-S directions obtained in the upper and lower reservoirs, respectively, of oilfield IV, were confirmed by previous studies, and admitted to be caused by dextral basement strike-slip faulting system, recognized in the Arabian Gulf (Edgell, 1992; Sirat et al.,

2007). Seismic interpretation and outcrop analysis conducted by Sirat (2015), showed two slip fault and fracture patterns, the dominant pattern is oriented N 75° W and the minor one is oriented NW-SE. Fractures with the dominant orientation were formed earlier in a short period, when SHmax (maximum horizontal stress) orientation was oriented approximately 120° with respect to the north direction. Fractures oriented along NW-SE direction were formed later as a result of the reactivation of the preexisting N 75° W by an SHmax oriented E-W (Sirat, 2015). Salahuddin et al. (2017) interpreted core data collected from ten wells drilled in oilfield III and confirmed the two patterns.

The findings of this study show the potential of this cost-effective multicomponent S-wave velocity analysis method, in detecting fractures in geological reservoirs and obtaining their orientation. We suggest the implementation of this analysis as a routine for fractures analysis along with other techniques such as core and FMI interpretation. This cost-effective technique can be used for investigating selected sites for $CO_2$ sequestration and energy storage.

## 7. Conclusions

We have investigated fractured carbonate reservoirs using the shear-wave splitting concept, by applying the multicomponent shear-wave velocity analysis. The analysis is based on the use of differently polarized shear events at given depth intervals, in order to obtain apparent velocities and preferential fracture strikes. The application of this cost-effective analysis, on synthetic and field data attest the ability of analyzing the shear-wave splitting phenomenon, and hence extracting the preferential fracture strike in Abu Dhabi reservoirs, from near zero-offset 3C VSP data. This analysis is less sensitive to the overburden anisotropy and random signal noise. We recommend the implementation of such analysis along with the well logging routines to obtain fracture properties at seismic scale.

## Acknowledgements

We are grateful for the excellent research collaboration between Khalifa University of Science and Technology and ADNOC and its operating companies, for providing access to the necessary material and data.

## Conflict of interest

The authors declare no competing interest.



## References

Ali, M. Y., Aidarbayev, S., Searle, M. P., et al. Subsidence history and seismic stratigraphy of the western musandam peninsula, oman-united arab emirates mountains. Tectonics, 2018, 37(1): 154-181.

Ali, M. Y., Bouchaala, F., Bouzidi, Y., et al. Integrated fracture characterization of thamama reservoirs in Abu Dhabi oil field, United Arab Emirates. SPE Reservoir Evaluation and Engineering, 2021, 24(4): 708-720.

Ali, M. Y., Sirat, M., Small, J. Geophysical investigation of Al Jaww Plain, eastern Abu Dhabi: Implications for structure and evolution of the frontal fold belts of the Oman Mountains. GeoArabia, 2008, 13(2): 91-118.

Ali, M. Y., Watts, A. B., Searle, M. P. Seismic stratigraphy and subsidence history of the United Arab Emirates (UAE) rifted margin and overlying foreland basins, in Lithosphere Dynamics and Sedimentary Basins: The Arabian Plate and Analogues, edited by K. Al Hosani, F. Roure, R. Ellison, et al., Springer, Berlin, Heidelberg, pp. 127-143, 2013.

Bakulin, A., Grechka, V., Tsvankin, I. Estimation of fracture parameters from reflection seismic data-Part I: HTI model due to a single fracture set. Geophysics, 2000, 65(6): 1788-1802.

Bale, R., Gratacos, B., Mattocks, B., et al. Shear wave splitting applications for fracture analysis and improved imaging: Some onshore examples. First Break, 2009, 27(9): 32448.

Bohlen, T. Parallel 3-D viscoelastic finite-difference seismic modelling. Computers & Geosciences, 2002, 28(8), 887-899.

Bouchaala, F., Ali, M. Y., Matsushima, J. Detailed study of seismic wave attenuation from four oilfields in Abu Dhabi, United Arab Emirates. Journal of Geophysics and Engineering, 2018, 15(1): 106-120.

Bouchaala, F., Ali, M. Y., Matsushima, J., et al. Azimuthal investigation of compressional seismic-wave attenuation in a fractured reservoir. Geophysics, 2019, 84(6): B437-B446.

Bouchaala, F., Guennou, C. Estimation of viscoelastic attenuation of real seismic data by use of ray tracing software: Application to the detection of gas hydrates and free gas. Comptes Rendus Géoscience, 2012, 344(2): 57-66.

Chopra, S., Marfurt, K. Curvature attribute applications to 3D surface seismic data. The Leading Edge, 2007, 26(4): 404-414.

Crampin, S., Peacock, S. A review of the current understanding of seismic shear-wave splitting in the earth's crust and common fallacies in interpretation. Wave Motion, 2008, 45(6): 675-722.

Ding, P., Wang, D., Li, X. An experimental study on scale-dependent velocity and anisotropy in fractured media based on artificial rocks with controlled fracture geometries. Rock Mechanics and Rock Engineering, 2020, 53(7): 3149-3159.

Ding, P., Wei, J., Di, B., et al. Observation and theoretical calibration of the fluid flow mechanism of artificial porous rocks with various size fractures. Geophysical Prospecting, 2021, 69(6): 1235-1247.

Edgell, H. S. Basement tectonics of saudi arabia as related to oil field structures, in Basement Tectonics 9, edited by M. J. Rickard, H. J. Harrington, P. R. Williams, Springer, Berlin, Heidelberg, pp. 169-193, 1992.

Gao, D., Di, H. Extreme curvature and extreme flexure analysis for fracture characterization from 3D seismic data: New analytical algorithms and geologic implications.

Geophysics, 2015, 80(2): IM11-IM20.

Hale, D. Methods to compute fault images, extract fault surfaces, and estimate fault throws from 3D seismic images. Geophysics, 2013, 78(2): O33-O43.

Jaglan, H., Qayyum, F., Hélène, H. Unconventional seismic attributes for fracture characterization. First Break, 2015, 33(3): 79520.

Johnson, C., Hauge, T., Al-Menhali, S., et al. Structural styles and tectonic evolution of onshore and offshore Abu Dhabi, UAE. Paper IPTC 10646 Presented at International Petroleum Technology Conference, Doha, Qatar, 21-23 November, 2005.

Landa, E., Keydar, S., Kravtcov, A. Determination of a shallow velocity-depth model from seismic refraction data by coherence inversion. Geophysical Prospecting, 1995, 43(2): 177-190.

Li, X., Ali, S. 3dvsp processing report zakum development compnay (zadco). Schlumberger SIS-Data Services, 2016.

Mandal, A., Srivastava, E. Enhanced structural interpretation from 3D seismic data using hybrid attributes: New insights into fault visualization and displacement in Cretaceous formations of the Scotian Basin, offshore Nova Scotia. Marine and Petroleum Geology, 2018, 89(2): 464-478.

Marfurt, K. J., Kirlin, R. L., Farmer, S. L., et al. 3-D seismic attributes using a semblance-based coherency algorithm. Geophysics, 1998, 63(4): 1150-1165.

Matsushima, J., Ali, M. Y., Bouchaala, F. A novel method for separating intrinsic and scattering attenuation for zero-offset vertical seismic profiling data. Geophysical Journal International, 2017, 211(3): 1655-1668.

Miyazawa, M., Snieder, R., Venkataraman, A. Application of seismic interferometry to extract P-and S-wave propagation and observation of shear-wave splitting from noise data at Cold Lake, Alberta, Canada. Geophysics, 2008, 73(4): D35-D40.

Muttoni, G., Gaetani, M., Kent, D. V., et al. Opening of the Neo-Tethys Ocean and the Pangea B to Pangea A transformation during the Permian. GeoArabia, 2009, 14(4): 17-48.

Noufal, A. Characteristics of salt-related faults in Abu Dhabi, UAE. Paper SPE 202605 Presented at Abu Dhabi International Petroleum Exhibition & Conference, Abu Dhabi, UAE, 9-12 November, 2020.

Patton, T., O'connor, S. Cretaceous flexural history of northern Oman Mountain foredeep, United Arab Emirates. AAPG Bulletin, 1988, 72(7): 797-809.

Pevzner, R., Gurevich, B., Urosevic, M. Estimation of azimuthal anisotropy from vsp data using multicomponent S-wave velocity analysis. Geophysics, 2011, 76(5): D1-D9.

Richard, P., Zampetti, V., Volery, C., et al. Abu Dhabi structural evolution and its implications for exploration. Paper SPE 188973 Presented at Abu Dhabi International Petroleum Exhibition & Conference, Abu Dhabi, UAE, 13-16 November, 2017.

Salahuddin, A. A., Qureshi, Z. U., Bandyopadhyay, I., et al. Utilization of geosciences, geostatistics, and fluid flow simulations to evaluate well placement sensitivity. Paper SPE 186076 Presented at SPE Reservoir Characterisation and Simulation Conference and Exhibition, Abu Dhabi, UAE, 8-10 May, 2017.

Searle, M. Thrust tectonics of the Dibba zone and the structural evolution of the Arabian continental margin along the Musandam mountains (Oman and United Arab Emirates). Journal of the Geological Society, 1988, 145(1): 43-53.

Searle, M. P. Structural geometry, style and timing of deformation in the Hawasina Window, Al Jabal al Akhdar and Saih Hatat culminations, Oman Mountains. GeoArabia, 2007, 12(2): 99-130.

Searle, M. P., Cherry, A. G., Ali, M. Y., et al. Tectonics of the Musandam Peninsula and northern Oman Mountains: From ophiolite obduction to continental collision. GeoArabia, 2014, 19(2): 135-174.

Simm, R., Bacon, M. Seismic Amplitude: An Interpreter's Handbook. Cambridg, UK, Cambridge University Press, 2014.

Sirat, M. Regional stress rotation in arabia; implications for hydrocarbon E&P in Abu Dhabi, UAE. Paper SPE 175604 Presented at SPE Reservoir Characterisation and Simulation Conference and Exhibition, Abu Dhabi, UAE, 14-16 September, 2015.

Sirat, M., Salman, S., Bellah, S. Fracturing mechanism and fracture systems analysis of carbonate reservoir from Abu Dhabi, UAE. Paper SPE 111397 Presented at SPE/EAGE Reservoir Characterization and Simulation Conference, Abu Dhabi, UAE, 28-31 October, 2007.

Skeith, G., Obara, T., El-Awawdeh, R., et al. Improved fracture characterization by utilizing seismic-derived attributes including anisotropy and diffraction imaging in a giant offshore carbonate field, UAE. Paper SPE 177597 Presented at Abu Dhabi International Petroleum Exhibition and Conference, Abu Dhabi, UAE, 9-12 November, 2015.

Takougang, E. M. T., Ali, M. Y., Bouzidi, Y., et al. Characterization of a carbonate reservoir using elastic full-waveform inversion of vertical seismic profile data. Geophysical Prospecting, 2020, 68(6): 1944-1957.

Tsuji, T., Hino, R., Sanada, Y., et al. In situ stress state from walkaround VSP anisotropy in the kumano basin southeast of the Kii Peninsula, Japan. Geochemistry, Geophysics, Geosystems, 2011, 12(9): Q0AD19.

WiMann, H., Rathjens, C., Kossmat, F. 1. Beiträge zur Tektonik Arabiens. Geologische Rundschau, 1943, 33(4-6): 221-353.

Zhao, L., Yao, Q., Han, D., et al. Characterizing the effect of elastic interactions on the effective elastic properties of porous, cracked rocks. Geophysical Prospecting, 2016, 64(1): 157-169.